The 1,2,3-Tridehydrobenzene Triradical: ^{2}B or Not ^{2}B? The Answer is ^{2}A!

Lucas Koziol,[†] Michael Winkler,*[,‡] K.N. Houk,[‡] Sugumar Venkataramani,[§] Wolfram Sander,[§] and Anna I. Krylov*[,†]

Department of Chemistry, University of Southern California, Los Angeles, California 90089-0482, Department of Chemistry and Biochemistry, University of California, Los Angeles, California 90095-1569, and Lehrstuhl für Organische Chemie II der Ruhr-Universität Bochum, Universitätsstrasse 150, 44780 Bochum, Germany

Received: February 20, 2007; In Final Form: March 31, 2007

The molecular and electronic structure of 1,2,3-tridehydrobenzene was investigated by a variety of computational methods. The two lowest electronic states of the triradical are the $^2B_2$ and $^2A_1$ doublet states characterized by different interactions of the unpaired electrons. Vertically, the two states are well separated in energy—by 4.9 and 1.4 eV, respectively. However, due to different bonding patterns, their equilibrium structures are very different and, adiabatically, the two states are nearly degenerate. The adiabatic energy gap between the $^2B_2$ and $^2A_1$ states is estimated to be 0.7−2.1 kcal/mol, in favor of the $^2A_1$ state. Harmonic vibrational frequencies and anharmonic corrections were calculated for both states. Comparison with the three experimentally observed IR transitions supports the assignment of the $^2A_1$ ground state for the triradical with a weakly bonding distance of 1.67−1.69 Å between the meta radical centers.

1. Introduction

Triradicals[1] are of fundamental interest due to their complex electronic structure and unusual bonding patterns arising from the interaction of three formally unpaired electrons. The electronic structures of the phenyl radical and the three benzyne isomers, which are formally derived from benzene by removal of two hydrogen atoms, have been the subject of many investigations.[2−10] However, tridehydrobenzenes **1**−**3** (Figure 1), the next step in the systematic decomposition of benzene (as discussed by Wenthold),[11] are characterized less extensively. Their increased multiconfigurational character challenges both theory and experiment.

Previous theoretical studies by Krylov and co-workers[1,12,13] demonstrated that the unpaired electrons form partial bonds between the radical centers, with stabilizing interactions ranging from 0.5 to 32 kcal/mol.[13] All three isomers possess low-spin doublet ground states. The doublet-quartet splitting is largest in 1,2,3-tridehydrobenzene (**1** in Figure 1), which indicates strongest interaction between adjacent radical sites. Isomers **2** and **3** are less stable than **1** by approximately 2.5 and 17.3 kcal/mol, respectively. These values are in agreement with heats of formation experimentally determined in gas phase by Wenthold and co-workers.[14,15]

Recently, Sander and co-workers reported the preparation and infrared (IR) spectroscopic characterization of **1** isolated in cryogenic neon matrices at 3 K (Figure 2).[16] 1,2,3-Tridehydrobenzene was prepared by photolysis of 3-iodophthalic anhydride **4** resulting in formation of monoradical **5** and benzyne **6**. Upon subsequent short-wavelength irradiation, produced a species with three characteristic absorptions at 524, 753, and 1698 cm^{-1} (among other side-products). Upon annealing the matrix at 8 K, recombination with iodine atoms was observed, leading to the disappearance of the three absorptions and formation of **6** (at the same time, the concentration of precursor **4** increased at the expense of **5**).

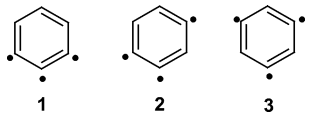

Figure 1. The three isomers of tridehydrobenzenes.

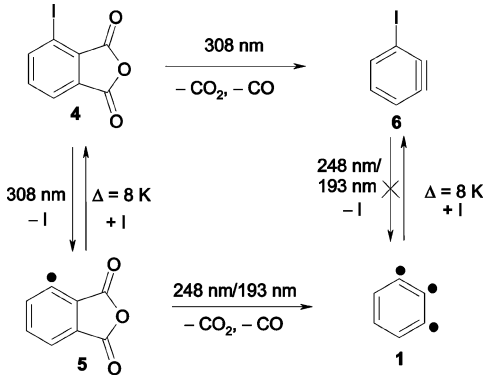

Figure 2. Matrix isolation of 1,2,3-tridehydrobenzene. Compound **4** was photolyzed with 308 nm light using an XeCl excimer laser. Subsequent irradiation with 248 nm KrF or 193 nm ArF excimer lasers produced **1**, as well as other side products.

Although the two lowest doublet states of 1,2,3-tridehydrobenzene, $^2A_1$ and $^2B_2$ (Figure 3), are well separated in energy *vertically*,[13] they are nearly degenerate *adiabatically*, according to calculations by Sander and co-workers.[16] This large difference between the vertical and adiabatic gaps (see Figure 4) originates in different bonding patterns in the two states leading to significant geometric relaxation. The relative adiabatic ordering of the two states depends strongly on the methods employed and a weak preference (1−2 kcal/mol) for the $^2A_1$ state was obtained at higher levels of theory.[16] The two isomers are separated by a barrier of only 4−5 kcal/mol. By comparison of calculated and measured vibrational spectra, the matrix-isolated species was identified as $^2A_1$.

* To whom correspondence should be addressed. E-mail: krylov@usc.edu and michael.winkler@mail.ruhr-uni-bochum.de.
† University of Southern California.
‡ University of California, Los Angeles.
§ Universität Bochum.

10.1021/jp0714522 CCC: $37.00
Published on Web 05/23/2007

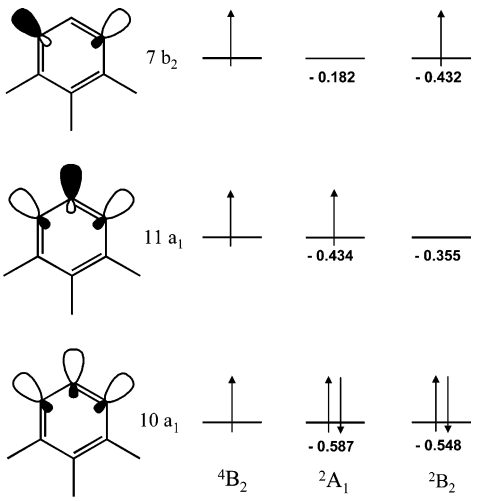

Figure 3. Frontier molecular orbitals and the leading electronic configurations of the $^4B_2$, $^2A_1$, and $^2B_2$ states of 1,2,3-tridehydrobenzene. Orbital energies (hartrees) for the UHF quartet reference are given at the optimized geometries of the two doublet states.

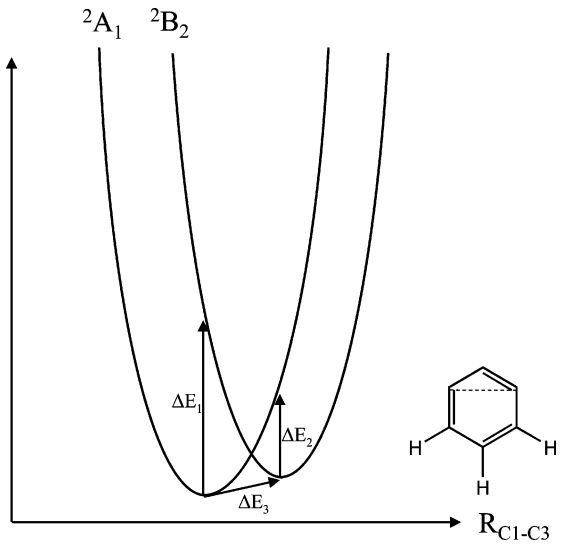

Figure 4. Vertical and adiabatic energy differences between the $^2A_1$ and $^2B_2$ states.

This contribution presents a series of high-level calculations aiming to quantify the $^2A_1-^2B_2$ splitting and to elucidate the electronic structure of the ground state of 1,2,3-tridehydrobenzene. Also, the measured IR data are compared to calculated vibrational spectra for both states at various levels of theory, including a discussion of anharmonic corrections at the BLYP/cc-pVTZ and B3LYP/cc-pVTZ levels. The structure of the paper is as follows. The next section outlines theoretical methods and computational details. Section 3 discusses equilibrium structures, vertical and adiabatic energy separations, and vibrational frequencies of the two states. Our final remarks are given in Section 4.

2. Theoretical Methods and Computational Details

Triradicals—species with three unpaired electrons distributed over three nearly degenerate orbitals—feature extensive electronic degeneracies that result in multi-configurational wave functions.[1] Similarly to diradicals,[17−20] the wave functions of low-spin states ($M_S = {}^1/_2$) are multi-determinantal, whereas the high-spin quartet state ($M_S = +{}^3/_2$) can be well described by a single-reference wave function. In general, these low spin states are not accessible by the traditional ground state single-reference methods, unless the energy gaps between the frontier MO are large enough to stabilize one of the determinants.

The $M_S = {}^1/_2$ states can be described by multireference methods employing a complete active space self-consistent field (CASSCF) reference wave function.[21] Dynamical electron correlation can be subsequently included by perturbation theory to second (RS2) or third (RS3) order,[22] or by truncated configuration interaction including single and double excitations (CISD) from the reference configurations.[23,24] In all CI calculations discussed in this work, internal contraction is applied to keep the number of configurations in the CI expansion manageable, whereas only the doubly external excitations are contracted in perturbation theory.[22] Due to the lack of size-consistency in truncated CI, the latter approach requires additional corrections, e.g., the Davidson correction, denoted as CISD+Q.[25] We also apply corrections inspired by the cluster expansion, i.e., the multireference average-quadratic coupled cluster (AQCC)[26] and multireference averaged coupled pair functional (ACPF) methods.[27]

Alternatively, all these states can be described accurately by the spin-flip (SF) models.[28−34] In the SF approach, low-spin states are described as spin-flipping excitations from a well-behaved high-spin reference state. In the case of triradicals, the SF method describes the target states as:

$$\Psi^{d,q}_{M_S=1/2} = \hat{R}_{M_S=-1}\tilde{\Psi}^{q}_{M_S=3/2} \qquad (1)$$

where $\tilde{\Psi}^{q}_{M_S=3/2}$ is the αααα high-spin reference determinant, e.g., $^4B_2$ from Figure 3, $\hat{R}_{M_S=-1}$ is an excitation operator that flips the spin of an electron ($\alpha \rightarrow \beta$), and $\Psi^{d,q}_{M_S=1/2}$ stands for the wave functions of the doublet and quartet target states. Because all the configurations (with $M_S = 1/2$) present in the low-lying triradical states are formally obtained from the $M_S = 3/2$ reference state by single excitations including a spin-flip, the SF method provides a balanced description of all the triradical states within a single-reference formalism.

An attractive feature of the SF approach is that non-dynamical and dynamical correlation are included in a single computational step. The description of the latter can be systematically improved by employing theoretical models of increasing complexity for the reference wave function.[28,30,32,33,35] In this work, we use a density-functional based method, SF-DFT, which was shown to yield accurate equilibrium structures and frequencies,[31,36] and two coupled-cluster based models:[33,35] equation-of-motion SF coupled-cluster with single and double substitutions [EOM-SF-CCSD or EOM-SF(2,2)], and the EOM-SF-CC method in which triple excitations are included in the EOM part, EOM-SF(2,3).

When the energy separations between the frontier orbitals are sufficiently large, the closed-shell doublet wave functions become single-determinantal and can also be well described by single-reference methods. The analysis of the $^2B_2$ and $^2A_1$ wave functions reveals that they are dominated by a single electronic configuration at the respective equilibrium geometries, i.e., the leading EOM-SF-CCSD amplitudes are 0.95 and 0.89 for the $^2A_1$ and $^2B_2$ states, respectively. This allows us to employ single-reference CCSD with perturbative inclusion of triple excitations, CCSD(T),[37,38] to calculate equilibrium geometries and vibrational frequencies of these states.

CCSD(T) calculations were performed using spin-unrestricted (UHF) and spin-restricted (ROHF) references. In the latter case, two different methods were employed: (i) ROHF-CCSD(T), which uses non spin-adapted cluster excitation operators $\hat{e}_{ai}$; and (ii) spin-adapted CCSD(T) [termed R-CCSD(T)], which

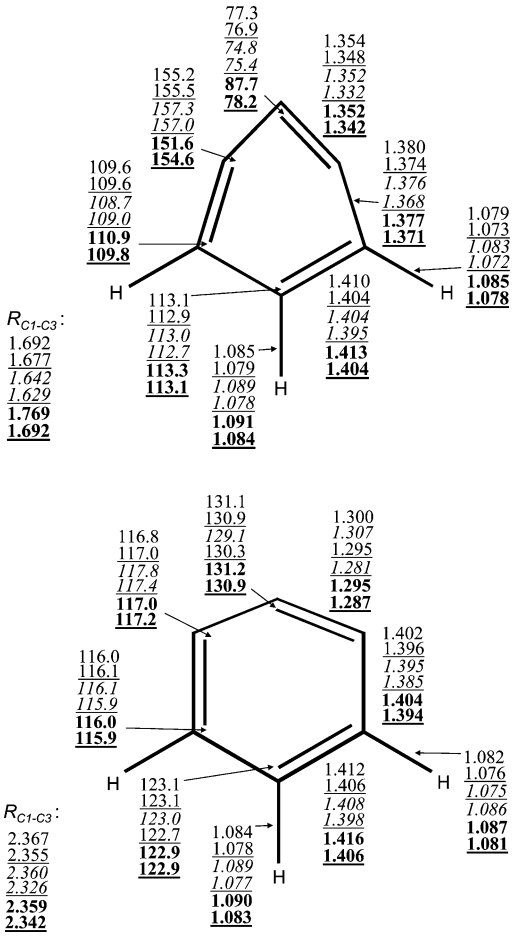

Figure 5. Equilibrium structure of the $^2A_1$ (upper panel) and $^2B_2$ (lower panel) states of 1,2,3-tridehydrobenzene. Bond lengths are in Angstroms and angles are in degrees.

R-CCSD(T)/cc-pVTZ
ROHF-CCSD(T)/cc-pVTZ
SF-CCSD/6-31G(d)
SF-DFT/6-311G(d)
BLYP/cc-pVTZ
B3LYP/cc-pVTZ

employs the spin-coupled operators $\hat{E}_{ai} = \hat{e}_{\bar{a}\bar{i}} + \hat{e}_{\bar{a}i}$, where tilde and overline refer to α and β spin orbitals, respectively (see ref 39). Although total energies are slightly different, the resulting structures, frequencies, and relative energies are very close. For instance, the adiabatic energy gap between the two lowest states is 0.026 eV (0.6 kcal/mol) lower in the ROHF-CCSD(T) calculation.

Equilibrium geometries and vibrational frequencies of these two low-lying states were calculated using the following methods: CCSD(T)[37,38] with cc-pVTZ basis,[40] SF-DFT[31] with 6-311G(d)[41] basis and a 50/50 functional (50% Hartree−Fock + 8% Slater + 42% Becke for exchange and 19% VWN + 81% LYP for correlation),[31] and B3LYP[42] with cc-pVTZ basis. The unrestricted $(10a_1)^1(7b_2)^1(11a_1)^1$ quartet reference was used for all spin-flip calculations. In CCSD(T) calculations, the ROHF reference was used in the optimization of the $^2A_1$ and $^2B_2$ states and UHF reference was employed in frequencies calculations. UHF-CCSD(T) geometries were also obtained, and are very similar to those obtained with the ROHF reference (bond lengths within 0.005 Å, angles within 0.01^o for $^2B_2$ and 0.5^o for $^2A_1$). Pure angular momentum spherical harmonics (5 d-functions) were used throughout. Single point CCSD(T)/cc-pVTZ calculations employed frozen core approximation for the lowest six orbitals.

CCSD, CCSD(T), and SF-CC single point energies were obtained at either EOM-SF-CCSD/6-31G(d) or ROHF-CCSD-(T)/cc-pVTZ optimized geometries. Effects of triple excitations were characterized by the EOM-SF(2,3) methods.

To approximate the energies of more expensive methods with large basis sets, an extrapolation scheme based on energy separability was used:

$$E^{\text{large}}_{EOM-SF(2,3)} = E^{\text{large}}_{EOM-SF(2,\tilde{3})} + (E_{EOM-SF(2,3)} - E_{EOM-SF(2,\tilde{3})})^{\text{small}} \quad (2)$$

$$E^{\text{large}}_{EOM-SF(2,3)} = E^{\text{large}}_{EOM-SF(2,2)} + (E_{EOM-SF(2,3)} - E_{EOM-SF(2,2)})^{\text{small}} \quad (3)$$

where E^{large} and E^{small} are total energies calculated in relatively large and small bases, respectively. This scheme assumes that changes in total energy due to basis set effects are similar for the different methods. In the EOM-SF(2,$\tilde{3}$) method, triple excitations are included only within a specified active space. This active space was chosen to include the three orbitals at the radical centers and the six benzene valence orbitals.

R-CCSD, R-CCSD(T), and multireference single point energies were also calculated by CAS-RS2, CAS-RS3, MR-CISD, AQCC, and ACPF using systematically larger basis sets (cc-pVDZ, cc-pVTZ, and cc-pVQZ) for both R-CCSD(T) and B3LYP/cc-pVTZ geometries. CASSCF calculations employed the same active space as in the EOM-SF(2,$\tilde{3}$) calculations, i.e., nine electrons in nine orbitals, CASSCF(9,9).

We also calculated anharmonic corrections to harmonic frequencies at the BLYP/cc-pVTZ and B3LYP/cc-pVTZ levels. Three methods were used: Transition-Optimized Shifted Hermite Theory (TOSH), vibrational perturbation theory (VPT2),[43] and vibrational configuration interaction (VCI).[44] In VPT2, the third and fourth power terms in the expansion of the potential are treated as perturbations, and the matrix elements of harmonic wave functions are computed. However, this method breaks down for near degenerate modes. In TOSH, the harmonic wave functions are shifted along the normal modes, by a distance σ. Comparing the first-order perturbation energy for this shifted wave function, with the second-order energy for the ordinary wave function, allows an approximation to σ that gives the second-order energy at only first-order cost. In VCI, the nuclear wave functions are expanded in the basis of a product of harmonic oscillators. VCI(n) refers to the inclusion of all basis functions in which the sum of excitations in all the modes is equal to n. Based on benchmark studies, VCI(1) and VCI(3) usually overestimate the true energy, whereas VCI(4) is close to the converged result.

At USC, calculations were performed using the Q-CHEM[45] and ACES II[46] electronic structure packages, whereas at UCLA and RUB the Gaussian03[47] and MOLPRO[48] packages were used.

3. Results and Discussion

3.1. Electronic Structure and Equilibrium Geometries of the $^2A_1$ and $^2B_2$ States. 1,2,3-Tridehydrobenzene, which is derived from benzene by removing three hydrogen atoms, has three adjacent sp^2-hybridized radical centers. Frontier molecular orbitals (MOs) and electronic configurations of the $^4B_2$, $^2A_1$, and $^2B_2$ states are shown in Figure 3. The leading electronic configurations are $(10a_1)^1(7b_2)^1(11a_1)^1$,$(10a_1)^2(11a_1)^1$, and $(10a_1)^2(7b_2)^1$, respectively. The two lowest electronic states of 1,2,3-

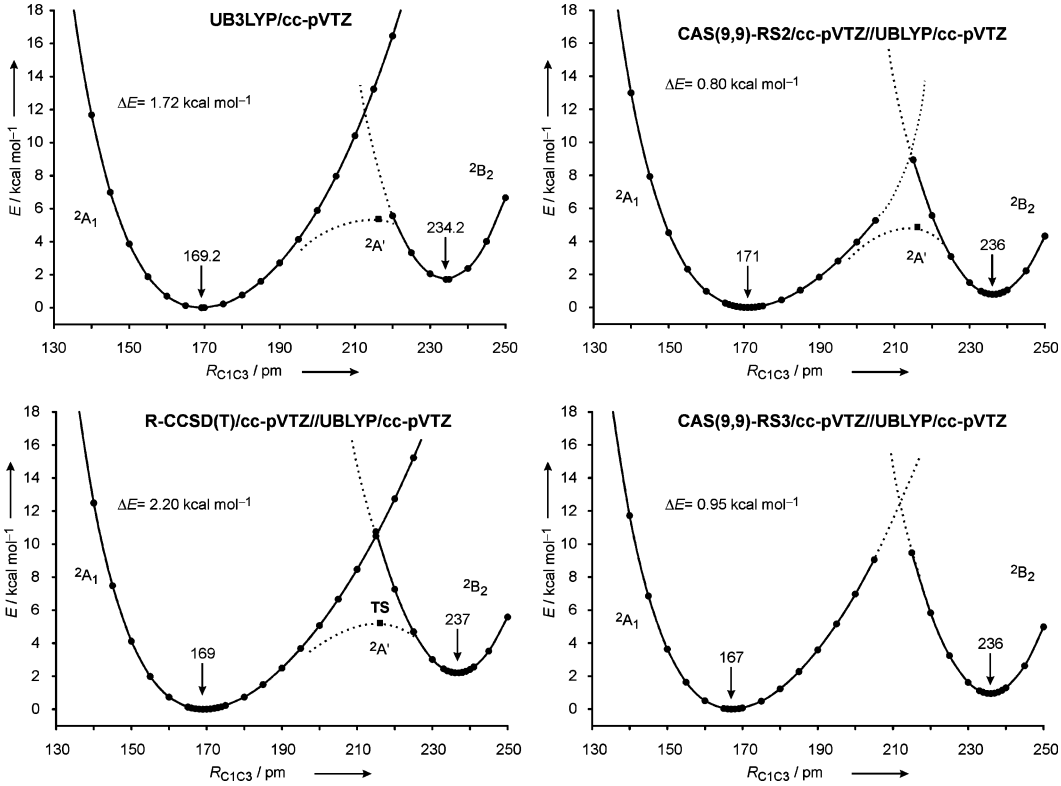

Figure 6. Energy as a function of the distance between the radical centers C1−C3.

TABLE 1: Selected Structural Parameters for the $^2A_1$ and $^2B_2$ Equilibrium Structures of 1 where R_{C1-C2} is the Bond Length between Adjacent Radical Carbons and $A_{C1-C2-C3}$ is the Angle Formed by the Three Radical Carbons

	$^2B_2$ state			$^2A_1$ state		
method	R_{1-3}, Å	R_{1-2}, Å	A_{1-2-3}, (deg)	R_{1-3}, Å	R_{1-2}, Å	A_{1-2-3}, (deg)
R-CCSD(T)/cc-pVTZ	2.367	1.300	131.1	1.692	1.354	77.3
ROHF-CCSD(T)/cc-pVTZ	2.355	1.295	130.9	1.677	1.348	76.9
EOM-SF-CCSD/6-31G(d)	2.361	1.307	129.1	1.642	1.353	74.8
SF-DFT/6-311G(d) 50/50 fnl	2.326	1.281	130.3	1.629	1.332	75.4
BLYP/cc-pVTZ	2.359	1.295	131.2	1.769	1.352	87.7
B3LYP/cc-pVTZ	2.342	1.287	130.9	1.692	1.342	78.2

tridehydrobenzene are closed-shell doublets with the bonding $10a_1$ orbital being doubly occupied (Figure 3). The states differ in the single occupation of either the $7b_2$ ($^2B_2$ state) or the $11a_1$ ($^2A_1$ state) orbitals.

The $10a_1$, $7b_2$, and $11a_1$ orbitals are of overall bonding, nonbonding, and antibonding character, respectively. Thus, the $^2B_2$ state, in which the bonding and nonbonding orbitals are occupied, appears to be a reasonable candidate for the ground state. However, the $11a_1$ orbital also has bonding character between the C1 and C3 radical centers, and this character increases upon benzene ring deformations that bring the two centers closer together. The competition between C1−C2−C3 and C1−C3 interactions results in the two states being nearly degenerate adiabatically.

The optimized geometries of the two doublet states are shown in Figure 5. They reveal large structural differences, in agreement with the characters of the corresponding MOs. With respect to the meta radical centers (C1 and C3), the $11a_1$ orbital is bonding, whereas the $7b_2$ orbital is antibonding. This leads to a contracted C1−C3 bond length (1.68−1.69 Å) in the $^2A_1$ state, as compared to 2.36−2.37 Å in the $^2B_2$ state. This bonding interaction in the $^2A_1$ state is much stronger than in singlet m-benzyne, where the corresponding distance is slightly above 2 Å.[13,49−51] The C1−C2 distance is longer by about 0.1 Å relative to o-benzyne (1.24 Å), reflecting the antibonding character of the occupied $11a_1$ orbital along these bonds. In the $^2B_2$ state, the C1−C2 distance is 1.30 Å, slightly longer than in o-benzyne, but shorter than in the $^2A_1$ state of **1**, showing that in this state the ortho- as well as meta- interaction is weaker than in the corresponding benzynes. The interaction of the three unpaired electrons in this state might therefore be called sigma allylic, in analogy with the nodal properties of the allyl system.

For well-behaved methods, e.g., CCSD(T) and SF, the structures of the two states are not very sensitive to the method used. Table 1 lists selected structural parameters obtained at various levels of theory. Despite a modest basis set, 6-31G(d), the EOM-SF-CCSD structures are in close agreement with the CCSD(T)/cc-pVTZ ones. Surprisingly, there are non-negligible differences between the two CCSD(T) methods. For bond lengths in well-behaved closed-shell molecules, the errors of the CCSD(T)/cc-pVTZ are about 0.008 Å (see ref 52). In the challenging case of the triradical, however, the differences in bond lengths calculated by the two CCSD(T) methods are of the same order, i.e., 0.006 and 0.015 Å for the C1−C2 and C1−C3 distances in the $^2A_1$ state.

Relative to CCSD(T)/cc-pVTZ, SF-DFT/6-311G(d) (with the 50/50 functional) slightly underestimates bond lengths and angles (by about 0.02 Å and 1°). BLYP/cc-pVTZ slightly overestimates them (by as much as 0.09 Å and 4° in the $^2A_1$ state), whereas B3LYP/cc-pVTZ yields slightly tighter structures, consistent with the presence of Hartree−Fock exchange. Overall, for the $^2A_1$ state, the B3LYP value for the C1−C3 bond

TABLE 2: Vertical and Adiabatic Energy Differences between the $^2A_1$ and $^2B_2$ States of 1,2,3-Tridehydrobenzene, as Defined in Figure 4 at EOM-CCSD/6-31G(d) Equilibrium Geometries unless Specified Otherwise

	method	ΔE_1[a], eV	ΔE_2[a], eV	ΔE_3[b], eV
1	EOM-SF-CCSD/6-31G	4.74	1.60	0.96
2	EOM-SF-CCSD/6-31G(d)	4.90	1.43	0.09
3	EOM-SF-CCSD/6-311G(d) (on C)	4.86	1.43	0.08
4	EOM-SF-CCSD/6-311G(2df)	4.86	1.43	0.08
5	EOM-SF(2,$\tilde{3}$)/6-31G	4.70	1.55	0.90
6	EOM-SF(2,3)/6-31G	4.71	1.55	0.89
7	EOM-SF(2,$\tilde{3}$)/6-31G(d)	4.84	1.43	0.003
8	EOM-SF(2,3)/6-31G(d)	4.85	1.43	−0.02
9	EOM-SF(2,3)/6-31G(d), extrapolated[c]	4.87	1.38	0.02
10	EOM-SF(2,3)/6-31G(d), extrapolated[d]	4.85	1.43	−0.01
11	EOM-SF(2,3)/6-311G(2df), extrapolated[e]	4.83	1.38	0.01
12	EOM-SF(2,3)/6-311G(2df), extrapolated[f]	4.81	1.43	−0.03
13	UHF-CCSD/cc-pVTZ			−0.17
14	ROHF-CCSD/cc-pVTZ			−0.17
15	UHF-CCSD(T)/cc-pVTZ			−0.26
16	ROHF-CCSD(T)/cc-pVTZ			−0.07
17	ΔZPE[g]			0.006

[a] Absolute value. [b] $E(^2B_2) - E(^2A_1)$. Negative values correspond to $^2A_1$ ground state. [c] EOM(2,3)/6-31G(d)≈EOM(2,2)/6-31G(d)+[EOM(2,3)-EOM(2,2)]$_{6-31G}$. [d] EOM(2,3)/6-31G(d)≈EOM(2,$\tilde{3}$)/6-31G(d)+[EOM(2,3)-EOM(2,$\tilde{3}$)]$_{6-31G(d)}$. [e] EOM(2,3)/6-311G(2df)≈EOM(2,2)/6-31G(2df)+[EOM(2,3)-EOM(2,2)]$_{6-31G}$. [f] EOM(2,3)/6-311G(2df) ≈ EOM(2,2)/6-31G(2df)+[EOM(2,3)-EOM(2,2)]$_{6-31G(d)}$. [g] At UHF-CCSD(T)/cc-pVTZ level.

TABLE 3: Adiabatic Energy Difference ΔE_3, eV, at R-CCSD(T)/cc-pVTZ and B3LYP/cc-pVTZ Equilibrium Geometries; All Multireference Calculations Employ a CASSCF(9,9) Reference

method	cc-pVDZ	cc-pVTZ	cc-pVQZ
R-CCSD[a]	−0.22	−0.23	−0.22
R-CCSD[b]	−0.22	−0.23	−0.23
R-CCSD(T)[a]	−0.10	−0.10	−0.09
R-CCSD(T)[b]	−0.09	−0.10	−0.09
CASSCF[a]	0.66	0.68	0.68
CASSCF[b]	0.69	0.71	0.71
CAS-RS2[a]	−0.02	−0.03	−0.04
CAS-RS2[b]	−0.01	−0.03	−0.04
CAS-RS3[a]	−0.03	−0.04	−0.05
CAS-RS3[b]	−0.02	−0.04	−0.05
MR-CISD[a]	0.18	0.20	0.20
MR-CISD[b]	0.20	0.21	0.22
MR-CISD+Q[a]	0.00	0.01	0.01
MR-CISD+Q[b]	0.02	0.02	0.02
AQCC[a]	0.00	0.00	0.00
AQCC[b]	0.01	0.00	0.00
ACPF[a]	−0.03	−0.03	−0.03
ACPF[b]	−0.02	−0.03	−0.03

[a] B3LYP/cc-pVTZ equilibrium geometry. [b] R-CCSD(T)/cc-pVTZ equilibrium geometry.

lengths agrees with CCSD(T) better than the BLYP one, whereas for the C1−C2 bond in the $^2B_2$ state the opposite is true. Relatively strong dependence of DFT geometries on the fraction of Hartree−Fock exchange is common in open-shell species and systems with vibronic interactions and has been rationalized in terms of the self-interaction error.[53,54]

Following our earlier studies on *m*-benzynes,[49−51] we also calculated PES scans along the reaction coordinate connecting the two minima, as sketched in Figure 4. This is done by constraining the C1−C3 distance (at intervals of ±0.01 Å around the minimum energy structures), and optimizing all other degrees of freedom at the DFT level. Subsequently, higher-level calculations were carried out at these geometries (Figure 6). Regarding the C1−C3 equilibrium distance, the R-CCSD(T) structure (1.69 ± 0.01 Å compared to 1.692 Å in full optimization) is nicely flanked by the CAS-RS2 (1.71 ± 0.01 Å) and CAS-RS3 (1.67 ± 0.01 Å) distances.

Our most reliable ROHF-CCSD(T)/cc-pVTZ and R-CCSD(T) estimates of the distance between the meta radical centers in $^2B_2$ and $^2A_1$ are 2.355−2.367 Å and 1.677−1.692 Å, respectively.

TABLE 4: CCSD(T)/cc-pVTZ Frequencies and IR Intensities

	$^2A_1$ state			$^2B_2$ state		
symmetry	frequency	I	I_{rel}	frequency	I	I_{rel}
$1a_1$	474	31	36	579	1	1
$2a_1$	823	1	1	841	3	4
$3a_1$	1079	3	3	1038	0	0
$4a_1$	1103	1	1	1130	13	18
$5a_1$	1436	4	5	1431	1	1
$6a_1$	1803	45	52	1577	0	0
$7a_1$	3201	9	10	3195	1	1
$8a_1$	3273	1	1	3237	7	10
$1a_2$	603	0	0	460	0	0
$2a_2$	827	0	0	921	0	0
$1b_1$	391	1	1	448	0	0
$2b_1$	598	1	1	590	2	3
$3b_1$	805	87	100	800	72	100
$4b_1$	980	1	1	993	0	0
$1b_2$	550	64	74	433	21	29
$2b_2$	923	11	13	1120	1	1
$3b_2$	1101	8	9	1143	10	14
$4b_2$	1301	1	1	1283	0	0
$5b_2$	1323	12	14	1370	7	10
$6b_2$	1545	12	14	1492	1	1
$7b_2$	3269	1	1	3229	3	4

TABLE 5: SF-DFT/6-311G* Frequencies and IR Intensities

	$^2A_1$ state			$^2B_2$ state		
symmetry	frequency	I	I_{rel}	frequency	I	I_{rel}
$1a_1$	539	42	27	625	1	1
$2a_1$	857	2	1	893	3	3
$3a_1$	1107	2	1	1069	0	0
$4a_1$	1133	0	0	1165	16	19
$5a_1$	1491	6	4	1496	1	1
$6a_1$	1886	32	20	1649	0	0
$7a_1$	3287	11	7	3278	2	2
$8a_1$	3339	2	1	3305	13	15
$1a_2$	555	0	0	468	0	0
$2a_2$	791	0	0	939	0	0
$1b_1$	432	6	4	445	1	1
$2b_1$	645	2	1	601	3	3
$3b_1$	875	157	100	798	86	100
$4b_1$	999	0	0	1006	1	1
$1b_2$	611	49	31	435	23	27
$2b_2$	951	8	5	1158	5	6
$3b_2$	1130	7	4	1203	5	6
$4b_2$	1344	1	1	1350	1	1
$5b_2$	1386	9	6	1402	4	5
$6b_2$	1600	9	6	1544	4	5
$7b_2$	3335	1	1	3298	10	12

3.2. Vertical and Adiabatic Energy Differences between the $^2A_1$ and $^2B_2$ States. Figure 4 defines the vertical and adiabatic energy separations of the two states. The corresponding values for the vertical electronic energies ΔE_1 and ΔE_2, and

TABLE 6: BLYP/cc-pVTZ Harmonic and Fundamental Vibrational Frequencies for the Two Doublet States of 1

	$^2A_1$ state				$^2B_2$ state			
symmetry	harmonic	TOSH	VPT2	VCI(2)	harmonic	TOSH	VPT2	VCI(2)
$1a_1$	412	403	402	410	569	550	545	555
$2a_1$	810	802	803	808	817	804	804	809
$3a_1$	1042	1021	1011	1028	994	983	982	988
$4a_1$	1050	1037	1038	1043	1094	1082	1080	1091
$5a_1$	1375	1347	1335	1354	1369	1344	1330	1352
$6a_1$	1715	1683	1693	1692	1519	1503	1510	1516
$7a_1$	3081	2901	2904	2944	3092	2826	2877	2929
$8a_1$	3147	3000	3001	3065	3116	2954	2966	2995
$1a_2$	550	545	546	550	431	438	435	444
$2a_2$	772	785	593	810	833	853	733	871
$1b_1$	359	325	268	334	384	380	362	388
$2b_1$	557	549	548	554	535	548	534	556
$3b_1$	735	710	543	737	729	726	568	748
$4b_1$	898	826	684	850	910	897	813	913
$1b_2$	519	512	499	520	437	432	377	449
$2b_2$	894	867	872	875	1092	1056	1041	1067
$3b_2$	1081	1044	1027	1053	1143	1124	1125	1134
$4b_2$	1258	1229	1212	1237	1260	1230	1212	1242
$5b_2$	1323	1288	1283	1300	1390	1337	1317	1350
$6b_2$	1474	1435	1428	1444	1475	1397	1433	1439
$7b_2$	3144	2913	2984	2967	3109	2865	2932	2921

TABLE 7: B3LYP/cc-pVTZ Frequencies, IR Intensities, and Anharmonic Corrections[a]

	$^2A_1$ state					$^2B_2$ state				
symmetry	ν_{harm}	I	I_{rel}	ν_{anharm}	$\Delta\nu$	ν_{harm}	I	I_{rel}	ν_{anharm}	$\Delta\nu$
$1a_1$	471	27	33	452	−19	448	0	0	441	−6
$2a_1$	829	1	1	818	−10	883	0	853	0	−30
$3a_1$	1070	4	5	1047	−24	1121	9	13	1107	−15
$4a_1$	1086	1	1	1064	−22	1122	14	20	1101	−20
$5a_1$	1423	4	5	1390	−34	1424	5	8	1400	−25
$6a_1$	1784	37	45	1708	−77	1562	0	0	1510	−52
$1a_2$	581	0	0	570	−11	584	2	2	562	−22
$2a_2$	802	0	0	787	−15	847	3	4	825	−21
$1b_1$	367	0	0	362	−5	416	1	1	408	−8
$2b_1$	581	2	2	571	−10	563	3	5	551	−11
$3b_1$	772	82	100	756	−16	766	70	100	748	−18
$4b_1$	950	0	0	930	−19	1027	0	0	1007	−19
$1b_2$	548	65	79	535	−13	469	31	45	456	−14
$2b_2$	916	9	11	892	−23	964	0	0	944	−21
$3b_2$	1098	4	5	1081	−17	1167	4	6	1142	−26
$4b_2$	1294	1	1	1265	−29	1300	1	1	1277	−23
$5b_2$	1346	6	8	1302	−45	1418	0	0	1385	−33
$6b_2$	1522	14	17	1482	−40	1512	1	1	1475	−38

[a] Anharmonic force constants up to quartic order were obtained by finite differences of Cartesian Hessians, for terms with up to three distinct indices.[58]

for the adiabatic energy difference ΔE_3, are listed in Tables 2 and 3. The ZPE correction is given separately and is not included in ΔE's.

The vertical energy gaps between the two states are fairly consistent for all levels of theory, and rather large: at the $^2A_1$ geometry (ΔE_1), the states are separated by 4.8 eV, and at the $^2B_2$ (ΔE_2) geometry by 1.4 eV. However, the adiabatic difference (ΔE_3) is much smaller due to geometrical relaxation, and the two states are nearly degenerate.

In contrast to ΔE_1 and ΔE_2, ΔE_3 depends strongly on the basis set employed in the calculation. Regardless of method, 6-31G yields an adiabatic energy difference of about 0.9 eV. Inclusion of polarization functions at carbon atoms is necessary, which lowers ΔE_3 to 0.1 eV or less. Increasing from double-ζ to triple-ζ basis, e.g., 6-31G(d) → 6-311G(d), has a comparatively small effect (0.01 eV). The effect of additional polarization, e.g., 6-311G(d) → 6-311G(2df), is also minor. Overall, for this system the EOM-SF method is converged at 6-31G(d).

All EOM-SF(2,2) calculations place the $^2B_2$ below the $^2A_1$ state, but the latter is less stable by only 0.1 eV or less with polarized basis sets. Inclusion of triples further brings the $^2A_1$ energy down relative to $^2B_2$. Restricting triple excitations to an active space (the three singly occupied and six π and π^* orbitals) at 6-31G(d) results in adiabatic difference of about 0.003 eV. Full triple excitations at the 6-31G(d) level predict $^2A_1$ to be 0.02 eV more stable than the $^2B_2$ state.

The systematic effect of partial and full triples on ΔE_3 suggests taking advantage of extrapolation schemes, eqs 2 and 3, to approximate the effect of full triples in the large basis set limit. Within a given basis set, the inclusion of active space triples affects ΔE_3 significantly, whereas full triples provide only a smaller additional correction. For example, with the 6-31G basis set, the active space triples lower ΔE_3 by 0.06 eV relative to EOM-SF(2,2), whereas full triples contribute an additional 0.01 eV. With the 6-31G(d) basis set, EOM-(2, $\tilde{3}$) lowers ΔE_3 by 0.09 eV, whereas EOM-(2,3) contributes an additional 0.02

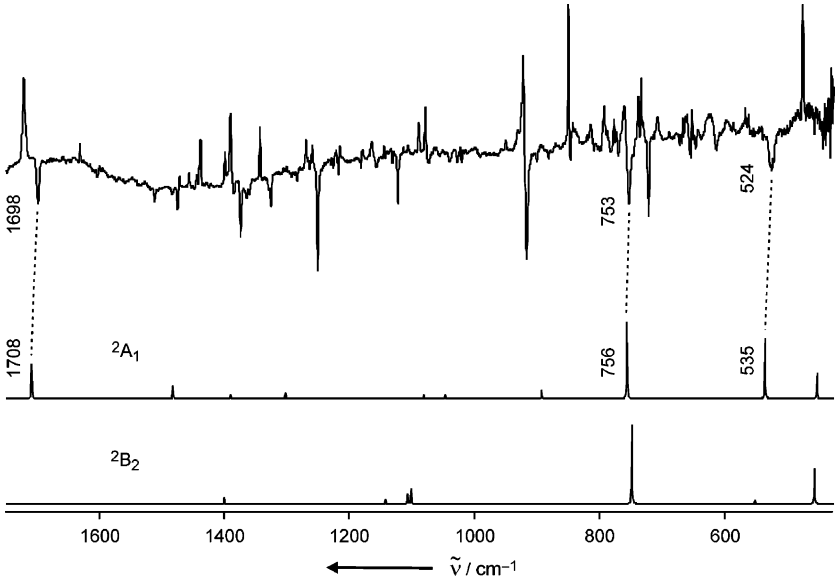

Figure 7. Experimental IR spectrum of **1** compared to B3LYP/cc-pVTZ calculated spectra for the $^2A_1$ and $^2B_2$ states, including anharmonic corrections.

eV. Although absolute values of ΔE_3 are very different (0.9 vs 0.1 eV), this similarity indicates that (i) active space triples sufficiently account for most of the correlation provided by full triples, and (ii) this effect is fairly consistent across different basis sets. In terms of energy separability, eq 2 provides a better extrapolation scheme than eq 3, yielding a very accurate result for ΔE_3 in the 6-31G → 6-31G(d) example (within 0.01 eV, see entries 8 and 10 in Table 2).

The EOM-SF(2,3)/6-311G(2df) energy was extrapolated using the calculated EOM-SF(2,2)/6-311G(2df) value and the difference between the EOM(2,3) and EOM(2,2) values with the 6-31G(d) basis set (eq 3). This gives −0.03 eV, or −0.69 kcal/mol, for ΔE_3. Lowering by 0.03 eV to account for the difference between active and full space triples schemes yields a final approximated EOM-SF(2,3)/6-311G(2df) ΔE_3 of −0.06 eV, or −1.38 kcal/mol. The ROHF-CCSD(T)/cc-pVTZ and R-CCSD(T) energy differences are −0.07 and −0.10 eV, or −1.61 and −2.3 kcal/mol, respectively. Both CCSD(T) methods agree very well with each other. Moreover, the excellent agreement between these two very different approaches, CCSD(T) and EOM-SF(2,3), is very encouraging. Both methods include triple excitations. CCSD(T) is very accurate for systems with single configurational wave functions, whereas EOM-SF-CCSD gives a balanced description of a general triradical wave function, both in the limit of small and large energy separations between the frontier MOs.

In addition to R-CCSD and R-CCSD(T) data, Table 3 summarizes results of multireference calculations. Whereas Hartree−Fock, which systematically overestimates bonding interactions, places $^2A_1$ significantly below $^2B_2$ (see Ref[16]), CASSCF overestimates the contributions of antibonding configurations and reverses the state ordering. In both cases, inclusion of dynamical correlation brings the two states closer in energy. Multireference perturbation theory to second or third order gives $\Delta E_3 = -0.05$ eV, in agreement with the EOM(2,3) and CCSD(T) results. Multireference CI approaches yield larger discrepancies. MR-CISD still favors the $^2B_2$ state by as much as 0.20−0.22 eV, whereas the Davidson correction leads to a nearly vanishing energy gap, indicating that size-extensivity effects are significant for a proper description of the relative energy of the two doublet states. The Davidson-corrected gaps are in agreement with almost perfect degeneracy predicted by AQCC. ACPF, which is considered to be a particularly suitable compromise between multireference and size-extensivity effects, returns to a moderate preference of 0.03 eV for the $^2A_1$ state.

Using different equilibrium geometries [R-CCSD(T) vs B3LYP], as well as basis sets beyond cc-pVTZ have negligible effect on adiabatic energy gaps. The inclusion of zero point energies provides a minor correction of 0.006 eV. To summarize, the best estimate of the adiabatic energy difference between the two states (including ZPE) is 0.03−0.09 eV, or 0.69−2.07 kcal/mol. Based on numerous benchmark studies,[52,55,56] the conservative estimate of the error bar for our ΔE_3 is ±1 kcal/mol, or about 0.02 eV.

3.3. Vibrational Spectrum. The three experimentally observed absorptions at 1698, 753, and 524 cm^{-1} have been assigned to the $^2A_1$ ground state of the title triradical, based on a comparison with spectra calculated at the BLYP/cc-pVTZ level for both states.[16] Although two lower frequencies are reproduced reasonably well for both states, the third intense line, 1698 cm^{-1}, is absent in the $^2B_2$ state, which was a decisive argument in favor of $^2A_1$. According to these calculations, the fourth and fifth most intense absorptions of **1** in the $^2A_1$ state are around 399 and 1467 cm^{-1} with rather low relative intensities of 17 and 18%, respectively.

To further complete the IR spectrum of **1**, refined measurements in the mid-IR region, as well as FIR measurements down to 200 cm^{-1}, have been carried out. No additional signals that could unequivocally be assigned to the tridehydrobenzene were identified in these spectral ranges, however.

On the computational side, we conducted a series of calculations aimed to refine theoretical frequencies and, most importantly, to establish error bars for the theoretical predictions. Due to the open-shell character of the triradical, the benchmark results obtained for the closed-shell molecules[52] are not directly transferable. Moreover, anharmonicities and possible matrix-induced shifts further complicate the comparison with the experiment. The rest of this section presents our analysis of harmonic frequencies calculated by DFT, SF-DFT, and CCSD(T), as well as anharmonic corrections evaluated by the VPT2, VCI, and TOSH approaches using DFT potential energy surfaces.

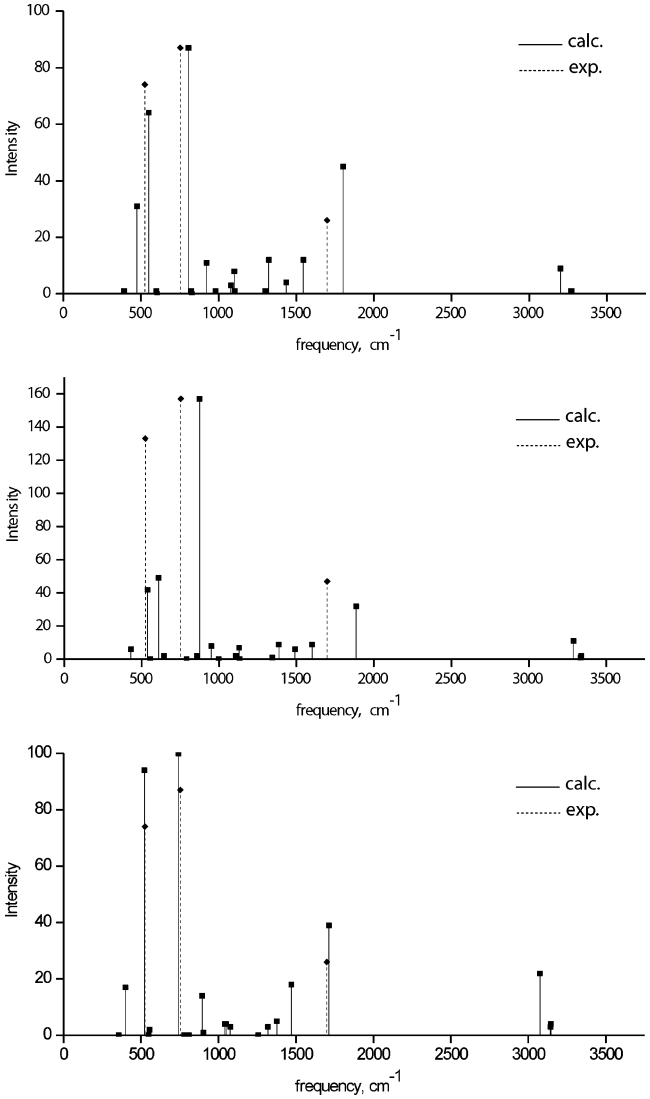

Figure 8. Calculated frequencies for the $^2A_1$ state (solid lines) compared to the three experimental absorptions (dashed lines). The intensities of the lines are scaled such that the intensities of the most intense experimental and calculated peaks are equal. Top: CCSD(T)/cc-pVTZ; middle: SF-DFT/6-311G(d) with 50/50 functional; bottom: BLYP/cc-pVTZ.

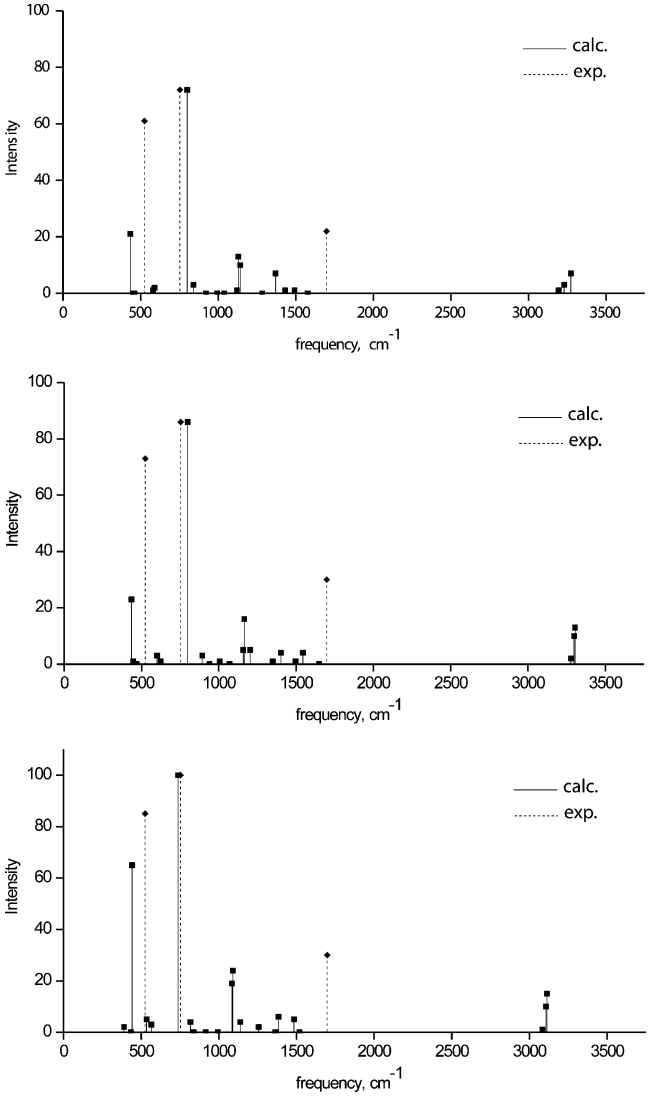

Figure 9. Calculated frequencies for the $^2B_2$ state (solid lines) compared to the three experimental absorptions (dashed lines). The intensities of the lines are scaled such that the intensities of the most intense experimental and calculated peaks are equal. Top: CCSD(T)/cc-pVTZ; middle: SF-DFT/6-311G(d) with 50/50 functional; bottom: BLYP/cc-pVTZ.

Calculated harmonic frequencies and anharmonic corrections for the $^2A_1$ and $^2B_2$ states are summarized in Tables 4−7, and compared with experimental data in Figures 7−9. Results are given for: CCSD(T)/cc-pVTZ, SF-DFT/6-311G(d) with 50/50 functional, BLYP with VPT2, VCI2, and TOSH anharmonicities, and B3LYP/cc-pVTZ with VPT2 anharmonic corrections. Among the electronic structure methods, CCSD(T) frequencies are expected to be the most accurate. For well-behaved systems, CCSD(T)/cc-pVTZ harmonic frequencies are within 2% (based on benchmark studies of diatomics) of the experimental values, which translates into 11, 15, and 34 cm^{-1} error bars for the three strongest transitions. However, comparison with experiment is not straightforward due to anharmonicities. Typical anharmonic corrections are about 2% of the harmonic frequencies (e.g., see a benchmark study of diatomics[57]), although anharmonicities of 3−5 % are rather common, yielding a correction of about 15−30 cm^{-1} for a 500 cm^{-1} harmonic mode. Moreover, anharmonicities may mix normal modes and significantly alter intensities.

Vibrational frequencies for the $^2A_1$ state are shown in Figure 8. The strongest (most intense) calculated peak lies within 6.5% of the strongest experimental peak, for both states and all methods except SF-DFT/6-311G(d) (which shows a 14% difference for the $^2A_1$ state). For all methods, the most intense absorption corresponds to an out-of-plane (b_1) wagging mode of the three hydrogens. All methods also reproduce the experimentally observed band at 1698 cm^{-1}, to the $^2A_1$ state which is an a_1 breathing mode of the three radical carbons. The deviations from experiment are 5.8, 9.9, and 0.6% for CCSD(T), SF-DFT, and anharmonically corrected B3LYP frequencies, respectively.

The lowest frequency peak, experimentally observed at 524 cm^{-1}, cannot be definitely assigned by the calculations. At the CCSD(T) and SF-DFT levels, two modes of sizable intensity are calculated within the close energy region: the $1a_1$ and $1b_2$ modes, both in-plane deformations of the carbon skeleton with large amplitudes on the meta radical centers. At the CCSD(T) level, the $1b_2$ mode (at 550 cm^{-1}) is within 4.7% of the experimental frequency and comparable in relative intensity. However, the $1a_1$ mode (at 474 cm^{-1}) is within 9.5% and also has considerable (though less than the $1b_2$) intensity.

At the SF-DFT level, both low-frequency modes shift to higher frequencies: the $1a_1$ mode, at 539 cm^{-1}, is slightly higher than experiment, and the $1b_2$ is at 611 cm^{-1}. This contradicts the CCSD(T) results.

Frequencies for the $^2B_2$ state are shown in Figure 9. The two low-frequency modes are similar for both studies with all methods. However, the third peak at 1698 cm^{-1} is absent in all calculated spectra. There is a region around 400 cm^{-1} where one or two bands consistently appear with some intensity; however, no experimental peak is recorded within 350 cm^{-1}, or about 30%, of this frequency. Overall, the frequencies of this electronic state are much less sensitive to the method, compared to $^2A_1$.

Finally, to compare different treatments of anharmonicities, anharmonic corrections by several methods were calculated at the BLYP/cc-pVTZ level (see Table 6). Enormous corrections at the VPT2 level suggest the failure of this approach: for example, the frequencies at 735 and 772 cm^{-1} are both shifted by over 150 cm^{-1}. The TOSH and VCI(2) corrections are in relatively good agreement with experiment for all modes. For the $^2A_1$ state, TOSH gives an average correction of 3.1%, whereas VCI(2) gives a 1.8% correction. For the $^2B_2$ state, TOSH gives 2.2% correction, whereas VCI(2) gives only 0.6%.

With regard to anharmonically corrected BLYP frequencies, the VCI(2) results provide the best agreement with experiment. The two lower modes (at 519 and 735 cm^{-1}, harmonically) remain essentially unchanged. This is notable because these modes already closely reproduce experiment at the harmonic level. Moreover, the third mode (at 1715 cm^{-1}, harmonically) is corrected to 1692 cm^{-1}, very close to the experimental frequency (1698 cm^{-1}).

We also conducted B3LYP calculations of the harmonic frequencies and anharmonic corrections. Similarly to equilibrium geometries, B3LYP frequencies agree better than BLYP with the CCSD(T) values for the 3 most intense transitions ($6a_1$, $3b_1$, and $1b_2$). The BLYP frequencies for these modes are lower than the CCSD(T) ones by 88, 70, and 31 cm^{-1}, respectively, whereas the differences between B3LYP and CCSD(T) are only 19, 33, and 2 cm^{-1}. Relatively strong dependence of the DFT frequencies on the fraction of Hartree−Fock exchange is consistent with the observed trend for equilibrium structures discussed in Section 3.1 and is indicative of self-interaction error. Although the agreement between the calculated B3LYP anharmonic frequencies and the experiment is remarkable—they are within 10, 3, and 11 cm^{-1} of each other, the discrepancies between the CCSD(T) and DFT harmonic frequencies, as well as functional dependence, suggest more conservative estimates of the error bars of 10−30 cm^{-1}.

The fourth most intense absorption is calculated at 470 cm^{-1} (B3LYP and CCSD(T)). The anharmonic correction for this line is estimated to be 2−20 cm^{-1}. However, despite refined measurements in the IR and FIR regions, no signal in this spectral range could unequivocally be assigned to the triradical. Whether the calculated (harmonic) intensities for this mode are too high (at CCSD(T), SF-DFT, and DFT levels of theory), or whether the signal escapes detection for experimental reasons (e.g., line-broadening due to side-splitting), cannot be answered conclusively on the basis of the available data.

Nevertheless, the overall agreement of the three most intense experimentally observed absorptions with the high-level calculations described in this work, allows the matrix-isolated species to be identified as the $^2A_1$ ground state of the 1,2,3-tridehydrobenzene triradical, which is also supported by the calculated adiabatic energy differences between the two electronic states.

4. Conclusions

A variety of high-level quantum chemical methods were employed to characterize the two lowest electronic states of the 1,2,3-tridehydrobenzene triradical and to determine their relative energy. According to the nodal characteristics of the singly occupied molecular orbitals, the $^2A_1$ state of **1** shows a C1−C3 bonding interaction, with a distance between the formal radical centers around 1.68−1.69 Å, whereas this distance is much larger in the $^2B_2$ state (2.36−2.37 Å). As estimated by several correlated methods, the $^2A_1$ state is adiabatically 0.03−0.09 eV lower in energy. Assignment of the $^2A_1$ ground state is also supported by comparison of calculated vibrational frequencies with the measured matrix-IR spectrum of the molecule. The three absorptions assigned to the triradical are reproduced by *ab initio* and anharmonically corrected DFT calculations.

The extremely small energy gap between the $^2A_1$ and $^2B_2$ states suggests that the character of the ground state can be easily manipulated by introduction of appropriate substituents. In view of the different bonding patterns, the two electronic states of **1** are expected to differ considerably in their properties and reactivity. Investigations of substituted tridehydrobenzenes and attempts to understand substituent effects in these systems are currently in progress in our laboratories.

Acknowledgment. This work was conducted in the framework of the Center for Computational Studies of Electronic Structure and Spectroscopy of Open-Shell and Electronically Excited Species supported by the National Science Foundation through CRF:CRIF program. A.I.K. acknowledges the support from the Department of Energy. At RUB, this work was financially supported by the Deutsche Forschungsgemeinschaft and the Fonds der Chemischen Industrie. K.N.H. thanks the National Science Foundation (CHE-0548209) for financial support and computational facilities. M.W. thanks the Alexander von Humboldt-Foundation for a Feodor Lynen fellowship.

References and Notes

(1) Krylov, A. I. *J. Phys. Chem. A* **2005**, *109*, 10638.
(2) Wierschke, S. G.; Nash, J. J.; Squires, R. R. *J. Am. Chem. Soc.* **1993**, *115*, 11958.
(3) Squires, R. R.; Cramer, C. J. *J. Phys. Chem.* **1998**, *102*, 9072.
(4) Cramer, C. J.; Nash, J. J.; Squires, R. R. *Chem. Phys. Lett.* **1997**, *277*, 311.
(5) Bettinger, H. F.; Schleyer, P. v. R.; Schaefer, H. F., III. *J. Am. Chem. Soc.* **1999**, *121*, 2829.
(6) Sander, W. *Acc. Chem. Res.* **1999**, *32*, 669.
(7) Wenk, H. H.; Winkler, M.; Sander, W. *Angew. Chem.* **2003**, *115*, 518; *Angew. Chem., Int. Ed.* **2003**, *42*, 502.
(8) Crawford, T. D.; Kraka, E.; Stanton, J. F.; Cremer, D. *J. Chem. Phys.* **2001**, *114*, 10638.
(9) Wenthold, P. G.; Squires, R. R.; Lineberger, W. C. *J. Am. Chem. Soc.* **1998**, *120*, 5279.
(10) Radziszewski, J. G.; Nimlos, M. R.; Winter, P. R.; Ellison, G. B. *J. Am. Chem. Soc.* **1996**, *118*, 7400.
(11) Wenthold, P. *Angew. Chem., Int. Ed.* **2005**, *44*, 7170.
(12) Slipchenko, L. V.; Krylov, A. I. *J. Chem. Phys.* **2003**, *118*, 9614.
(13) Cristian, A. M. C.; Shao, Y.; Krylov, A. I. *J. Phys. Chem. A* **2004**, *108*, 6581.
(14) Lardin, H. A.; Nash, J. J.; Wenthold, P. G. *J. Am. Chem. Soc.* **2002**, *124*, 12612.
(15) Wenthold, P. G. Private communication.
(16) Venkataramani, S.; Winkler, M.; Sander, W. *Angew. Chem., Int. Ed.* **2005**, *44*, 6306.
(17) Borden, W. T. (Ed.) *Diradicals*; Wiley: New York, 1982.
(18) Salem, L.; Rowland, C. *Angew. Chem., Int. Ed. Engl.* **1972**, *11*, 92.
(19) Bonačić-Koutecký, V.; Koutecký, J.; Michl, J. *Angew. Chem., Int. Ed. Engl.* **1987**, *26*, 170.
(20) Slipchenko, L. V.; Krylov, A. I. *J. Chem. Phys.* **2002**, *117*, 4694.
(21) Roos, B. O. In *Ab initio methods in quantum chemistry, II*; John Wiley & Sons, New York, 1987; pp 399−446.

(22) Werner, H. *Mol. Phys.* **1996**, *89*, 645.
(23) Werner, H. J.; Knowles, P. J. *J. Chem. Phys.* **1988**, *89*, 5803.
(24) Knowles, P. J.; Werner, H. J. *Chem. Phys. Lett.* **1988**, *145*, 514.
(25) Langhoff, S. R.; Davidson, E. R. *Int. J. Quant. Chem.* **1974**, *8*, 61.
(26) Szalay, P. G.; Bartlett, R. J. *J. Phys. Chem.* **1995**, *103*, 3600.
(27) Gdanitz, R. J.; Ahlrichs, R. *Chem. Phys. Lett*. **1988**, *143*, 413.
(28) Krylov, A. I. *Chem. Phys. Lett*. **2001**, *338*, 375.
(29) Krylov, A. I. *Chem. Phys. Lett*. **2001**, *350*, 522.
(30) Krylov, A. I.; Sherrill, C. D. *J. Chem. Phys.* **2002**, *116*, 3194.
(31) Shao, Y.; Head-Gordon, M.; Krylov, A. I. *J. Chem. Phys.* **2003**, *118*, 4807.
(32) Sears, J. S.; Sherrill, C. D.; Krylov, A. I. *J. Chem. Phys.* **2003**, *118*, 9084.
(33) Levchenko, S. V.; Krylov, A. I. *J. Chem. Phys.* **2004**, *120*, 175.
(34) Krylov, A. I. *Acc. Chem. Res.* **2006**, *39*, 83.
(35) Slipchenko, L. V.; Krylov, A. I. *J. Chem. Phys.* **2005**, *123*, 84107.
(36) Vanovschi, V.; Krylov, A. I.; Wenthold, P. G. *Theor. Chim. Acta* **2007**, in press.
(37) Raghavachari, K.; Trucks, G. W.; Pople, J. A.; Head-Gordon, M. *Chem. Phys. Lett*. **1989**, *157*, 479.
(38) Watts, J. D.; Gauss, J.; Bartlett, R. J. *J. Chem. Phys.* **1993**, *98*, 8718.
(39) Knowles, P. J.; Hampel, C.; Werner, H. J. *J. Chem. Phys.* **1993**, *99*, 5219.
(40) Dunning, T. H. *J. Chem. Phys.* **1989**, *90*, 1007.
(41) Krishnan, R.; Binkley, J. S.; Seeger, R.; Pople, J. A. *J. Chem. Phys.* **1980**, *72*, 650.
(42) Becke, A. D. *J. Chem. Phys.* **1993**, *98*, 5648.
(43) Norris, L.; Ratner, M.; Roitberg, E.; Gerber, R. *J. Chem. Phys.* **1996**, *105*, 11261.
(44) Whitehead, R. J.; Handy, N. C. *J. Mol. Spect*. **1975**, *55*, 356.
(45) Shao, Y.; Molnar, L. F.; Jung, Y.; Kussmann, J.; Ochsenfeld, C.; Brown, S.; Gilbert, A. T. B.; Slipchenko, L. V.; Levchenko, S. V.; O'Neil, D. P.; Distasio, Jr. R. A.; Lochan, R. C.; Wang, T.; Beran, G. J. O.; Besley, N. A.; Herbert, J. M.; Lin, C. Y.; Van Voorhis, T.; Chien, S. H.; Sodt, A.; Steele, R. P.; Rassolov, V. A.; Maslen, P.; Korambath, P. P.; Adamson, R. D.; Austin, B.; Baker, J.; Bird, E. F. C.; Daschel, H.; Doerksen, R. J.; Drew, A.; Dunietz, B. D.; Dutoi, A. D.; Furlani, T. R.; Gwaltney, S. R.; Heyden, A.; Hirata, S.; Hsu, C.-P.; Kedziora, G. S.; Khalliulin, R. Z.; Klunziger, P.; Lee, A. M.; Liang, W. Z.; Lotan, I.; Nair, N.; Peters, B.; Proynov, E. I.; Pieniazek, P. A.; Rhee, Y. M.; Ritchie, J.; Rosta, E.; Sherrill, C. D.; Simmonett, A. C.; Subotnik, J. E.; Woodcock, H. L., III; Zhang, W.; Bell, A. T.; Chakraborty, A. K.; Chipman, D. M.; Keil, F. J.; Warshel, A.; Herhe, W. J.; Schaefer, III. H. F.; Kong, J.; Krylov, A. I.; Gill, P. M. W.; Head-Gordon, M. *Phys. Chem. Chem. Phys.* **2006**, *8*, 3172.
(46) Stanton, J. F.; Gauss, J.; Watts, J. D.; Lauderdale, W. J.; Bartlett, R. J. *ACES II*, 1993. The package also contains modified versions of the MOLECULE Gaussian integral program of Almlöf, J.; Taylor, P. R., the ABACUS integral derivative program written by Helgaker, T. U.; Jensen, H. J. Aa.; Jørgensen, P.; Taylor, P. R., and the PROPS property evaluation integral code of Taylor, P. R.
(47) Frisch, M. J.; Trucks, G. W.; Schlegel, H. B.; Scuseria, G. E.; Robb, M. A.; Cheeseman, J. R.; Montgomery, J. A., Jr.; Vreven, T.; Kudin, K. N.; Burant, J. C.; Millam, J. M.; Iyengar, S. S.; Tomasi, J.; Barone, V.; Mennucci, B.; Cossi, M.; Scalmani, G.; Rega, N.; Petersson, G. A.; Nakatsuji, H.; Hada, M.; Ehara, M.; Toyota, K.; Fukuda, R.; Hasegawa, J.; Ishida, M.; Nakajima, T.; Honda, Y.; Kitao, O.; Nakai, H.; Klene, M.; Li, X.; Knox, J. E.; Hratchian, H. P.; Cross, J. B.; Bakken, V.; Adamo, C.; Jaramillo, J.; Gomperts, R.; Stratmann, R. E.; Yazyev, O.; Austin, A. J.; Cammi, R.; Pomelli, C.; Ochterski, J. W.; Ayala, P. Y.; Morokuma, K.; Voth, G. A.; Salvador, P.; Dannenberg, J. J.; Zakrzewski, V. G.; Dapprich, S.; Daniels, A. D.; Strain, M. C.; Farkas, O.; Malick, D. K.; Rabuck, A. D.; Raghavachari, K.; Foresman, J. B.; Ortiz, J. V.; Cui, Q.; Baboul, A. G.; Clifford, S.; Cioslowski, J.; Stefanov, B. B.; Liu, G.; Liashenko, A.; Piskorz, P.; Komaromi, I.; Martin, R. L.; Fox, D. J.; Keith, T.; Al-Laham, M. A.; Peng, C. Y.; Nanayakkara, A.; Challacombe, M.; Gill, P. M. W.; Johnson, B.; Chen, W.; Wong, M. W.; Gonzalez, C.; Pople, J. A. *Gaussian 03*, revision C.02; Gaussian, Inc.: Wallingford, CT, 2004.
(48) Werner, H.-J.; Knowles, P. J.; Lindh, R.; Schütz, M.; et al. *MOLPRO 2002.6*, 2003.
(49) Winkler, M.; Sander, W. *J. Phys. Chem. A.* **2001**, *105*, 10422.
(50) Winkler, M.; Cakir, B.; Sander, W. *J. Am. Chem. Soc.* **2004**, *126*, 6135.
(51) Sander, W.; Exner, M.; Winkler, M.; Balster, A.; Hjerpe, A.; Kraka, E.; Cremer, D. *J. Am. Chem. Soc.* **2001**, *124*, 13072.
(52) Helgaker, T.; Jørgensen, P.; Olsen, J. *Molecular electronic structure theory*; John Wiley & Sons: New York, 2000.
(53) Polo, V.; Kraka, E.; Cremer, D. *Mol. Phys.* **2002**, *100*, 1771.
(54) Zhang, Y.; Yang, W. *J. Chem. Phys.* **1998**, *109*, 2604.
(55) Schuurman, M. S.; Muir, S. R.; Allen, W. D.; Schaefer, H. F. *J. Chem. Phys.* **2004**, *120*, 11586.
(56) Tajti, A.; Szalay, P. G.; Császár, A. G.; Kállay, M.; Gauss, J.; Valeev, E. F.; Flowers, B. A.; Vázquez, J.; Stanton, J. F. *J. Chem. Phys.* **2004**, *121*, 11599.
(57) Pawlowski, F.; Halkier, A.; Jorgensen, P.; Bak, K. L.; Helgaker, T.; Klopper, W. *J. Chem. Phys.* **2003**, *118*, 2539.
(58) Barone, V.; Minichino, C. *J. Molec. Struct. (THEOCHEM)* **1995**, *330*, 365.